On the impact of wind forcing on the seasonal variability of Weddell Sea Bottom Water transport

Q. Wang,[1] S. Danilov,[1] E. Fahrbach,[1] J. Schröter,[1] and T. Jung[1]

[1] The seasonal variability of Weddell Sea Bottom Water (WSBW) transport and its driving mechanisms are examined using FESOM simulations. Pronounced seasonal variability is present in both the Filchner shelf water export rate and the WSBW transport rate near the Antarctic Peninsula (AP) tip. The variabilities at both locations are linked to the surface wind forcing. The Filchner shelf water export rate responds to the onshore propagating density anomaly, which is caused by the wind-induced variation of the isopycnal depression at the coast. The variability near the AP tip originates from upstream variations at the Filchner Depression and from seasonal variability of the Weddell gyre strength. **Citation:** Wang, Q., S. Danilov, E. Fahrbach, J. Schröter, and T. Jung (2012), On the impact of wind forcing on the seasonal variability of Weddell Sea Bottom Water transport, *Geophys. Res. Lett.*, *39*, L06603, doi:10.1029/2012GL051198.

1. Introduction

[2] More than 60% of the Antarctic Bottom Water (AABW) is fed by Weddell Sea Deep Water (WSDW) [*Orsi et al.*, 1999]. Weddell Sea Bottom Water (WSBW, defined as bottom water with potential temperature below $-0.7°C$) is one of the main sources of the WSDW. WSBW has several sources along the Weddell Sea shelf regions, including the Ice Shelf Water (ISW) from the Filchner Depression (FD, see Figure 1a), the High Salinity Shelf Water (HSSW) from the southwestern Weddell Sea, and the ISW from the western shelf [*Fahrbach et al.*, 1995; *Gordon*, 1998; *Orsi et al.*, 1999; *Meredith et al.*, 2000; *Foldvik et al.*, 2004].

[3] Strong variability on both annual and interannual scales has been observed in the WSBW properties near the Antarctic Peninsula (AP) tip [*Fahrbach et al.*, 2001, hereinafter FB01] and southeast of the South Orkney Islands [*Gordon et al.*, 2010]. By examining the current velocity from moorings, FB01 suggest that the observed variations are due to fluctuations in WSBW formation rates and fluctuations related to the large-scale Weddell gyre circulation. *Gordon et al.* [2010] propose that the seasonal fluctuations of WSBW properties are governed by the seasonal cycle of winds over the western margin of the Weddell Sea. It is speculated that winds can influence both the production of HSSW and its access to the continental slope in the southwestern Weddell Sea, thus the bottom plume variability observed downstream [*Gordon et al.*, 2010; *McKee et al.*, 2011].

[4] In this work we use a numerical model with overflow-resolving resolution to study the seasonal variability of WSBW, with the focus on the bottom water originating from the FD. The driving mechanisms of the variability will be elucidated.

2. Model Setup

[5] The Finite Element Sea-ice Ocean Model (FESOM) [*Danilov et al.*, 2004; *Wang et al.*, 2008; *Timmermann et al.*, 2009] is used with a mesh refined along the main pathway of WSBW. The model domain covers the whole Southern Ocean south of 46°S. The horizontal resolution varies from 1° by 1°cos(latitude) in the bulk of the model domain to 2 km over the FD shelf region, the whole southern and western continental slope, and the northern limb of the Weddell gyre until about 30°W. This resolution is sufficient to represent the overflow eddies and the major small-scale topographic features which can be important in both steering and mixing [*Wang et al.*, 2009]. In the vertical, 48 sigma layers are used with refined thickness near the bottom. The model bottom topography is derived from the 1 min GEBCO data.

[6] The model is initialized with the hydrography from the World Ocean Atlas (WOA) 2001 [*Conkright et al.*, 2002]. Because the ISW in the FD is not properly represented in the WOA data, we prescribe the initial potential temperature and salinity in the FD following the transect observation by *Foldvik et al.* [1985a]. The potential temperature θ (salinity) is $-2.05°C$ (34.6 psu) below the 300 m depth, increasing (decreasing) linearly to $-1.9°C$ (34.5 psu) at the 200 m depth, and then to $-1.8°C$ (34.4 psu) at the 50 m depth. To facilitate the analysis of model results, a passive tracer with concentration $c = 1$ is injected into the ISW (with $\theta < -1.9°C$) in the FD. Salinity, θ, and c south of 76.5°S in the FD are restored during the simulation.

[7] The ocean is driven by the climatological wind forcing provided by *Large and Yeager* [2004]. It consists of 6 hourly wind velocity averaged over 43 years (1958–2000). The ocean temperature and salinity are restored to monthly climatology at the surface with a piston velocity of 10 m/5 days. At the northern open boundary they are restored to the initial data. The model was run for 10 years. First it was spun up for 4 years without applying the ISW source in the FD. Then the ISW source was switched on and the model was run for another 5 years. To further illustrate the role of surface wind, we turned off the wind forcing at the end of year 9 and ran the model for one year more. Figures 1b and 1c shows the time series of total volume transport at transects C and D (marked in Figure 1a), respectively. They reach a quasi-steady state between year 7 and 9. When we discuss the

[1]Alfred Wegener Institute for Polar and Marine Research, Bremerhaven, Germany.

(a)

(b)

(c)

(d)
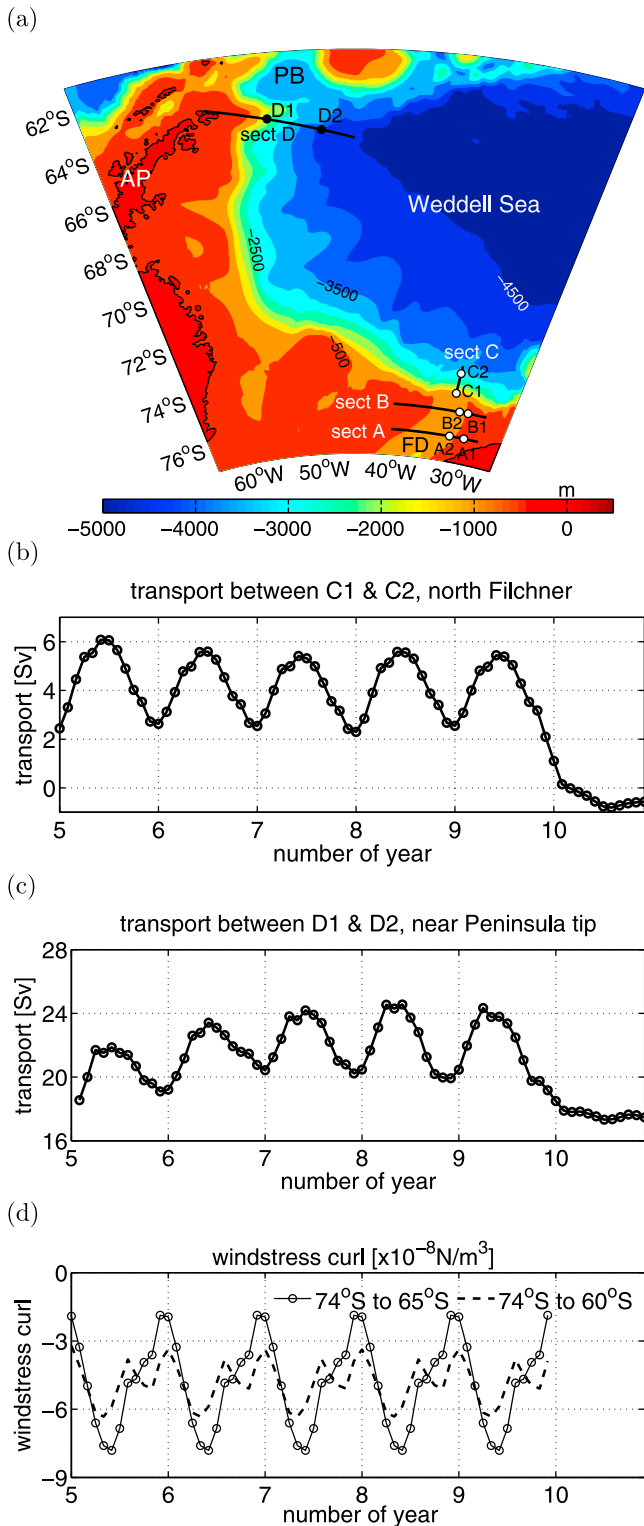
Figure 1. (a) Bathymetry of the Weddell Sea. FD, AP and PB stand for Filchner Depression, Antarctic Peninsula, and Powell Basin, respectively. Transects and sites mentioned in the text are labeled. (b) Total volume transport at transect C between sites C1 and C2. (c) The same as Figure 1b but for transect D between sites D1 and D2. (d) Wind stress curl averaged between 55°W and 50°W in longitude, and between 74°S and 60°S (65°S) in latitude. The x tick label is put at the location of January; the same for other figures.

mean seasonal cycle we deal with the average over this period.

3. Shelf Water Export From the FD

[8] The variability of the cyclonic Weddell gyre circulation is predominantly driven by surface wind forcing [*Lefebvre and Goosse*, 2005]. The total volume transport across transect C has a minimum in January and a maximum in June (Figure 1b). It has a similar phase at transect D, with a minimum between December and January, and a maximum between April and June. Their phase is anticorrelated with the mean wind stress curl in the Weddell-Enderby Basin (Figure 1d), illustrating the governing effects of wind forcing on the seasonal cycle of the Weddell gyre circulation.

[9] Figure 2a shows the time series of the total dense water export rate at the northern FD (transect A) and near to the sill (transect B), and their mean seasonal cycle. Unless otherwise specified, we use the criterion of $c > 0.1$ and $\theta < -0.7°C$ for calculating the transport. During year 5 the water mass over the shelf is clearly under adjustment, after which a quasi-steady seasonal cycle is observed. The annual mean export rate increases from 1 Sv at transect A to 1.1 Sv at transect B. This increase is mainly due to the mixing of the shelf water with surrounding water over the shelf, which is also reflected in the reduction of the ISW transport component between these two transects (calculated with $c > 0.1$, $\theta < -1.9°C$). The mean ISW transport is 0.93 and 0.82 Sv at transect A and B, respectively (not shown in figures).

[10] Only rough estimates for the shelf water export rate can be derived from observations. The ISW transport was estimated as 0.7 Sv by *Foldvik et al.* [1985b] and 1.6 Sv by *Foldvik et al.* [2004]. The difference is not due to interannual variability, but to the analysis approaches used. *Wilchinsky and Feltham* [2009] simulated the Filchner overflow with prescribed variable ISW influx ($0.5 - 2$ Sv) at the Filchner sill. The best fit to downstream mooring temperature observations was found with influxes of 0.5 and 1 Sv. Our simulation gives results inside this suggested range.

[11] The shelf water export rate has a peak in September and a minimum in austral summer (Figure 2a). This seasonal cycle is strongly anti-correlated with the density variability of the inflow water mass (red curve in Figure 3a, with a minimum in September and a maximum in January). The cold dense shelf water flows northward along the eastern side of the FD, while the coastal water flows southward adjacent to it at its eastern side (Details will be reported in another paper). The density gradient between the dense shelf water (on the west) and the light coastal water (on the east) produces bottom intensified shelf water outflow (on the west) and surface intensified coastal water inflow (on the east). The variability of the inflow density can thus modulate the outflow rate.

[12] At the coast, the phase of the density lags that of the coastal current transport (cf. Figures 1b and 3a). Stronger cyclonic wind and more intensive Weddell gyre circulation imply stronger depression of the isopycnal at the coast (lighter water at a fixed depth). However, they will not have exactly the same phase, as both the baroclinic adjustment and the water mass propagation along the coast take some time.
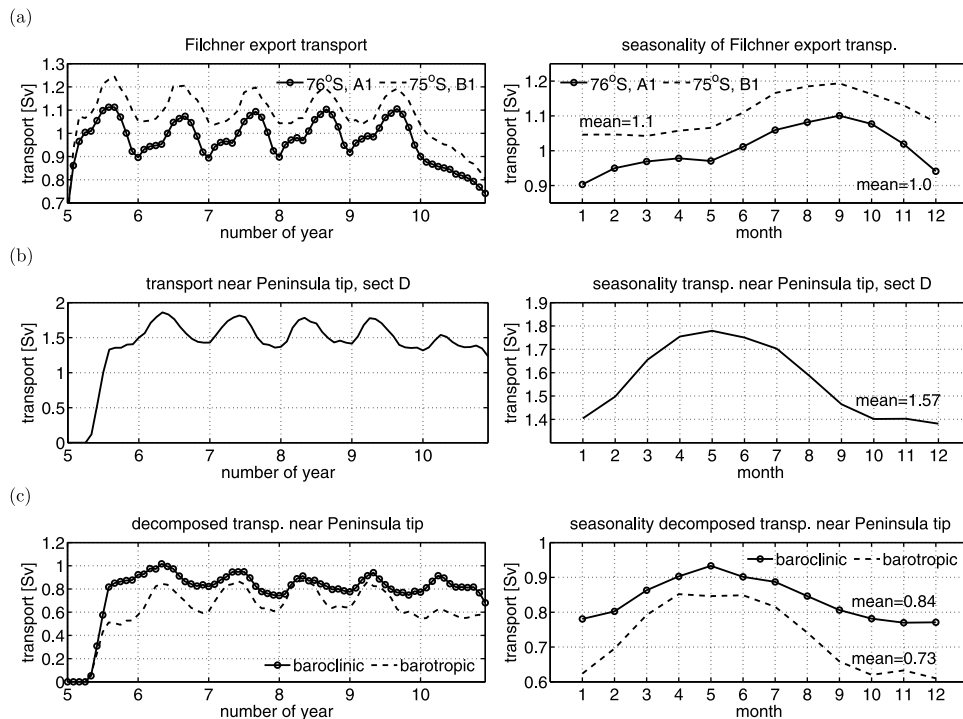
Figure 2. (a) Time series of the shelf water (left) export rate and (right) the mean seasonal cycle at transect A (solid) and B (dashed). (b) The same as Figure 2a but for the WSBW transport at transect D. (c) The same as Figure 2b but for decomposed WSBW transport. All time series are three months running mean; the same for plots in other figures.

[13] It takes about one month for the seasonal cycle pattern of the inflow density to propagate from the coast at C1 onshore to the northern FD at A1 (Figure 3a). This can be explained by advection. The inflow speed at the 100 m depth is about 5–12 cm/s over the 200 km distance between C1 and A1, corresponding to a propagation period between 19 and 46 days.

[14] Figure 3b shows the Hovmöller diagram of the potential density at 76°S in the southward inflow (A1) and northward outflow (A2). In the outflow, the water mass does not show significant variability except for the upper 50 m depth where the surface buoyancy forcing dominates. In the inflow the seasonal cycle is prominent over the column, although the variability is more pronounced over the upper 150 m depth. The variability of the outflow rate is linked to the net effect of the density anomaly over the column. We can use the density profiles at A1 and A2 to roughly estimate the relative variability of the outflow transport. Defining the anomaly of the outflow rate above the depth $H = 400$ m as δT, and the in situ density as ρ, we have $\delta T \sim -\int_H^0 \int_H^z (\rho_{A1} - \rho_{A2}) dz' dz$. After calculating δT, we subtract its mean and then divide it by its standard deviation. The same calculation is done for the sites B1 and B2 at 75°S. The result is shown in Figure 3c. The maximum of the derived transport anomaly is in August and September, and the minimum is in January and February. This is consistent with the phase in the directly calculated export rate (Figure 2a).

[15] In the last simulation year (year 10), the wind forcing is switched off and the coastal currents almost disappear at transect C (Figure 1b). There is no seasonal cycle in the density fields below about 50 m over the continental slope at C1 or over the shelf at B1 and A1 (Figures 3a and 3b). Therefore, the seasonal variability of the shelf water outflow is also absent (Figures 2a and 3c).

4. WSBW Transport Near the AP Tip

[16] Figure 2b shows the time series of the WSBW transport across transect D near the AP tip (Figure 1a) and its mean seasonal cycle. After the ISW was added in the FD at the beginning of year 5, it takes about 8 months for the WSBW transport to reach its mean level at this location. A pronounced seasonal cycle is present starting from year 6. The mean seasonal cycle shows a maximum transport in austral fall (around May) and a minimum in spring (from October to December). This agrees with FB01 who observed a similar seasonality. FB01 derived a mean WSBW transport of 1.3 ± 0.4 Sv between 1989 and 1998. The mean transport in our model is 1.57 Sv. There is considerable debate on the WSBW production rate estimated from observational data, with a range between 1–5 Sv [see, e.g., *Foldvik et al.*, 2004, Table 5]. Considering that we only have one WSBW source in the model, it is reasonable that the mean transport in our simulation is close to the lower bound of this range.

[17] To illustrate the impact of the Weddell gyre circulation on the transport at transect D, we decompose the WSBW transport into the baroclinic and barotropic components. When calculating the baroclinic transport, we subtracted the velocity at 400 m above the plume upper boundary at each column along the transect. This depth interval is chosen because the vertical shear of horizontal velocity at this level is close to the smallest value. The difference between the total plume transport and the baroclinic transport is defined as the barotropic transport in this
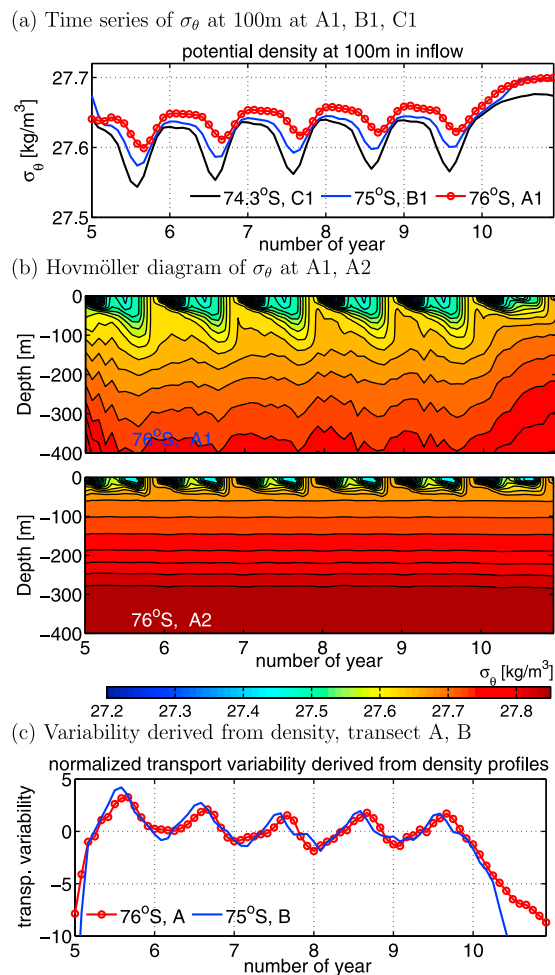
Figure 3. (a) Time series of potential density σ_θ at 100 m at sites A1, B1 and C1. (b) The Hovmöller diagram of σ_θ at sites A1 and A2. (c) Anomaly of the shelf water export rate derived from *in situ* density time series at transect A and B. See the text for the calculation method.

context. There is no absolute way to separate the baroclinic and barotropic components, thus we examined an alternative method by using the vertically averaged velocity as the barotropic velocity in each column. The seasonal variability of both components is nearly identical to the first calculation method (both the phase and magnitude of the anomaly), although the mean values of transport composition differ by about 0.1 Sv. Therefore, the separation of the two components is a reliable approach to demonstrate the composition of the variability.

[18] The transport components and their mean seasonal cycles are shown in Figure 2c. A clear seasonal cycle is present in both the baroclinic and barotropic transport components. They are in phase, with the maximum in austral fall and the minimum in austral spring. The magnitude of the seasonal variation is larger in the barotropic component. When the wind forcing is turned off during the last year, only the seasonal cycle of the baroclinic transport remains, while the magnitude of the barotropic transport anomaly reduces considerably (Figure 2c). At the end of year 10, the baroclinic transport is also clearly reduced, because the

signal of reduced export rate at FD (Figure 2a) has advected to this location.

[19] The seasonal cycle of the plume velocity (calculated by dividing the plume transport by the plume transect area) is shown in Figure 4a. It is in phase with the total plume transport (Figure 2b) and the plume velocity observed by FB01. The baroclinic and barotropic components of the plume velocity (Figure 4b) indicate that the barotropic velocity has much larger seasonal variability than the baroclinic counterpart. The plume area a across transect D has a seasonal cycle with a maximum in May and a minimum in October (Figure 4e). The observed seasonal phase of a by FB01 is similar to our model result, but their observed mean area (38 ± 5 km^2) is higher than in our simulation (25.5 km^2). We speculate that this is mainly due to the fact that we only specify one particular WSBW source (i.e., the ISW from the FD) in our model.

[20] We denote the temporal mean of the plume transect area as $[a]$, and its anomaly as a'. The same notation applies to the plume velocity v. The transport anomaly can be decomposed to three terms, $a'[v]$, $[a]v'$, and $a'v'$, which are shown in Figures 4c and 4d for the baroclinic and barotropic transport, respectively. The variability of the baroclinic transport is mainly due to the variability of the plume transect area, while both the variabilities of the barotropic velocity and plume transect area similarly contribute to the variability of barotropic transport. Consistent with the phase of the plume transport, velocity and area, the minimum bottom potential temperature is lowest in May (Figure 4f).

[21] The gyre circulation can influence the bottom plume upstream of the AP tip. The baroclinic component of the transport variability at transect D, contributed mainly from the plume transect area, already contains the accumulated impact from the wind driven gyre circulation. Therefore, the above diagnostics related to separating the barotropic and baroclinic components at transect D should be interpreted as an indication of the importance of wind forcing and gyre circulation, rather than a precise quantification of different contributions.

5. Conclusions

[22] Wind modulates the strength of the Weddell Sea coastal currents and the depth of isopycnals along the coast, thus the properties of the water mass that flows inshore adjacent to the FD outflow pathway. The seasonal cycle of the inflow density can lead to the variation of the shelf water export rate. This conclusion is supported by the recent theoretical study by *Kida* [2011].

[23] With only one WSBW source in our simulation, the observed WSBW variability near the AP tip is still reproduced. This can be considered as evidence supporting the suggestion of FB01: the wind induced variability in the gyre circulation over the bottom plume has very significant impact on the plume variability. Although the variability of shelf water export rates and the corresponding driving mechanisms in different regions (including the southern, southwestern and western Weddell Sea) can be different [e.g., *Gordon et al.*, 2010; *McKee et al.*, 2011], all contributions to WSBW can be similarly influenced by the barotropic gyre velocity along their propagation pathway, leading to the observed mean WSBW seasonality in the northern Weddell Sea: colder in austral fall and warmer in
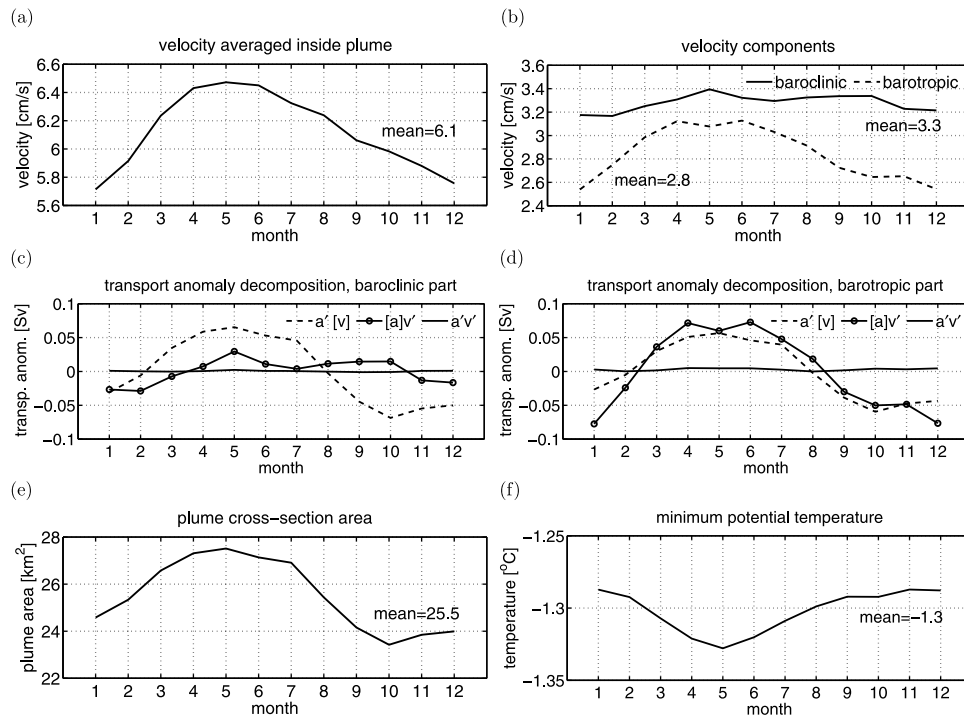
Figure 4. The mean seasonal cycle of (a) plume velocity, (b) decomposed baroclinic and barotropic plume velocity, (c) decomposed transport anomaly for the baroclinic component, (d) decomposed transport anomaly for the barotropic component, (e) plume transect area, and (f) minimum potential temperature at the plume bottom.

austral spring [FB01; *Gordon et al.*, 2010]. We speculate that the mechanisms driving the WSBW transport variability described in this paper also apply on interannual and longer time scales, which needs to be verified in future work.

References

Conkright, M., R. A. Locarnini, H. Garcia, T. O'Brien, T. Boyer, C. Stephens, and J. Antonov (2002), *World Ocean Atlas 2001: Objective Analyses, Data Statistics, and Figures, CD-ROM Documentation*, 17 pp., Natl. Oceanogr. Data Cent., Silver Spring, Md.

Danilov, S., G. Kivman, and J. Schröter (2004), A finite-element ocean model: Principles and evaluation, *Ocean Modell.*, 6, 125–150.

Fahrbach, E., G. Rohardt, N. Scheele, M. Schroder, V. Strass, and A. Wisotzki (1995), Formation and discharge of deep and bottom water in the northwestern Weddell Sea, *J. Mar. Res.*, 53, 515–538.

Fahrbach, E., S. Harms, G. Rohardt, M. Schroder, and R. A. Woodgate (2001), Flow of bottom water in the northwestern Weddell Sea, *J. Geophys. Res.*, 106, 2761–2778.

Foldvik, A., T. Gammelsrød, and T. Tørresen (1985a), Hydrographic observations from the Weddell Sea during the Norwegian Antarctic Research Expedition 1976/77, *Polar Res.*, 3, 177–193.

Foldvik, A., T. Gammelsrød, and T. Tørresen (1985b), Physical oceanography studies in the Weddell Sea during the Norwegian Antarctic Research Expedition 1978/79, *Polar Res.*, 3, 195–207.

Foldvik, A., T. Gammelsrød, S. Østerhus, E. Fahrbach, G. Rohardt, M. Schröder, K. W. Nicholls, L. Padman, and R. A. Woodgate (2004), Ice shelf water overflow and bottom water formation in the southern Weddell Sea, *J. Geophys. Res.*, 109, C02015, doi:10.1029/2003JC002008.

Gordon, A. L. (1998), Western Weddell Sea thermohaline stratification, in *Ocean, Ice and Atmosphere: Interactions at the Antarctic Continental Margin, Antarct. Res. Ser.*, vol. 75, edited by S. Jacobs and R. Weiss, pp. 215–240, AGU, Washington, D. C.

Gordon, A. L., B. Huber, D. McKee, and M. Visbeck (2010), A seasonal cycle in the export of bottom water from the Weddell Sea, *Nat. Geosci.*, 3, 551–556.

Kida, S. (2011), The impact of open oceanic processes on the Antarctic Bottom Water outflows, *J. Phys. Oceanogr.*, 41, 1941–1957.

Large, W. G., and S. G. Yeager (2004), Diurnal to decadal global forcing for ocean and sea-ice models: The data sets and flux climatologies, *NCAR Tech. Note NCAR/TN-460+STR*, 105 pp., Natl. Cent. for Atmos. Res., Boulder, Colo.

Lefebvre, W., and H. Goosse (2005), Influence of the Southern Annular Mode on the sea ice-ocean system: The role of the thermal and mechanical forcing, *Ocean Sci.*, 1, 145–157.

McKee, D. C., X. Yuan, A. L. Gordon, B. A. Huber, and Z. Dong (2011), Climate impact on interannual variability of Weddell Sea Bottom Water, *J. Geophys. Res.*, 116, C05020, doi:10.1029/2010JC006484.

Meredith, M. P., R. A. Locarnini, K. A. Van Scoy, A. J. Watson, K. J. Heywood, and B. A. King (2000), On the sources of Weddell Gyre Antarctic Bottom Water, *J. Geophys. Res.*, 105, 1093–1104.

Orsi, A. H., G. C. Johnson, and J. L. Bullister (1999), Circulation, mixing, and production of Antarctic Bottom Water, *Prog. Oceanogr.*, 43, 55–109.

Timmermann, R., S. Danilov, J. Schröter, C. Böning, D. Sidorenko, and K. Rollenhagen (2009), Ocean circulation and sea ice distribution in a finite element global sea ice-ocean model, *Ocean Modell.*, 27, 114–129.

Wang, Q., S. Danilov, and J. Schröter (2008), Finite element ocean circulation model based on triangular prismatic elements, with application in studying the effect of topography representation, *J. Geophys. Res.*, 113, C05015, doi:10.1029/2007JC004482.

Wang, Q., S. Danilov, and J. Schröter (2009), Bottom water formation in the southern Weddell Sea and the influence of submarine ridges: Idealized numerical simulations, *Ocean Modell.*, 28, 50–59.

Wilchinsky, A. V., and D. L. Feltham (2009), Numerical simulation of the Filchner overflow, *J. Geophys. Res.*, 114, C12012, doi:10.1029/2008JC005013.

S. Danilov, E. Fahrbach, T. Jung, J. Schröter, and Q. Wang, Alfred Wegener Institute for Polar and Marine Research, PO Box 12 01 61, D-27515 Bremerhaven, Germany. (sergey.danilov@awi.de; eberhard.fahrbach@awi.de; thomas.jung@awi.de; jens.schroeter@awi.de; qiang.wang@awi.de)